AIAA JOURNAL
Vol. 33, No. 7, July 1995

Viscous Airfoil Computations Using Adaptive Grid Redistribution

D. J. Hall* and D. W. Zingg†
University of Toronto, Downsview, Ontario M3H 5T6, Canada

A quantitative study of the numerical error reduction due to adaptive grid redistribution applied to Navier–Stokes computations of steady airfoil flows is presented. A grid redistribution procedure is described and applied to a range of flow cases including attached and separated flows at subsonic and transonic speeds. The error reduction resulting from grid adaptation is sensitive to the adaptive grid generation parameters used, especially those affecting the smoothness of the adapted grid. A suitable set of adaptive grid generation parameters is determined by comparison of adaptive grid solutions with grid-independent solutions. With the given parameters, adaptive grid redistribution is shown to result in an effective reduction in numerical error and improved resolution of flow features.

Introduction

THE effects of grid clustering and refinement on the prediction of lift and drag in thin-layer Navier–Stokes computations of steady airfoil flows were investigated in Ref. 1. This study demonstrated that very fine grids are required to reduce the numerical errors in both lift and drag to below 1%. Furthermore, the study showed that the characteristics of the grids required to achieve these error levels are strongly dependent on the features of the flow. These results provide motivation for solution-adaptive grids, both to increase the accuracy with a given number of grid points and to reduce the user expertise necessary to set up the grid.

Adaptation of grids is generally achieved either through adding and deleting points or redistributing existing points. The former approach, which includes both grid enrichment and grid embedding, generally leads to an unstructured database. Although the flexibility this provides is highly desirable for grid adaptation, flow solvers that use structured grids can be more efficient for simple geometries such as single-element airfoils. With adaptive grid redistribution, the original grid structure is retained, and flow solvers that require structured grids can be used. The relative advantages of the grid redistribution and grid embedding approaches are discussed by Dannenhoffer.[2]

In this paper, we examine the effectiveness of a grid redistribution scheme in reducing the numerical errors in Navier–Stokes computations of steady airfoil flows. Recent studies[3,4] have shown that the error reduction is highly dependent on the parameters used in grid adaptation schemes. Warren et al.[4] demonstrated that global error reduction is not guaranteed by fine resolution of flow features such as shock waves if adaptation parameters are not carefully selected. The objective of the present study is to determine a suitable set of grid adaptation parameters in the context of a specific application, viscous airfoil flows, and to examine the error reduction obtained through grid redistribution for a range of flow cases. A key aspect of the study is the use of the relatively grid-independent solutions computed in Ref. 1 to estimate the global error reduction produced by grid adaptation.

Errors in steady viscous airfoil computations result from physical model errors as well as numerical errors. Numerical errors are associated with the spatial discretization and include errors due to inadequate grid clustering, refinement, and smoothness, as well as excessive skewness and the position of the outer boundary. Numerical errors due to artificial dissipation are related to the spatial discretization since the effect of artificial dissipation is reduced as the grid is refined. Physical model errors include the thin-layer approximation and other approximations in the governing equations, prediction of the transition point and the process of transition, and the turbulence model. Although the physical model errors far exceed the numerical errors for many of the cases considered here, efficient reduction of numerical errors is important both to assess physical models and when improved physical models become available.

In the following sections, the adaptive redistribution method is described and the flow solver is briefly summarized. A description of test cases and grid characteristics follows. Parametric studies are then described from which an appropriate set of parameters is determined. Results are presented for a range of flow cases on different grids.

Adaptive Method

Redistribution schemes are generally implemented using either a control function, variational, or spring-analogy scheme. The control function method of Eiseman[5] is used for this study and has been used by several investigators.[2,6,7] In this method, control functions in a system of elliptic partial differential equations are used to cluster points in each coordinate direction. The control function method combines the inherent smoothness and limited skewness of elliptic systems with an adaptive redistribution capability. The adaptive control functions are combined with geometric control functions to allow certain geometric constraints to be specified at the boundaries.

Variational methods explicitly state the compromise between grid smoothness, orthogonality, and adaptation, but the resulting systems are quite complicated. Kim and Thompson[6] compared the control function method of Eiseman with the variational method of Brackbill and Saltzman[8] and found that the variational approach required more than three times the computational work of the control function approach. Holcomb[9] reported that the variational approach was unacceptable due to an inability to account for boundary point distributions, in contrast to the control function method. Although the spring-analogy method has been well developed and applied to various problems (see, for example, Davies and Venkatapathy[3]), the control function approach was selected due to its apparently superior smoothness and skewness attributes.

The adaptive method is summarized in the following text. The current implementation is described in detail in Ref. 10. Structured boundary-conforming grids are used in which a grid in the Cartesian x–y plane is considered to be a transformation from a uniform grid in the computational ξ–η plane where $\Delta\xi = \Delta\eta = 1$. The elliptic grid generation system is given by[11]

$$g_{22}(\boldsymbol{r}_{\xi\xi} + P\boldsymbol{r}_{\xi}) + g_{11}(\boldsymbol{r}_{\eta\eta} + Q\boldsymbol{r}_{\eta}) - 2g_{12}\boldsymbol{r}_{\xi\eta} = 0$$

where $\boldsymbol{r} = (x, y)$ is the Cartesian position vector and

$$g_{11} = \boldsymbol{r}_{\xi} \cdot \boldsymbol{r}_{\xi}, \qquad g_{12} = \boldsymbol{r}_{\xi} \cdot \boldsymbol{r}_{\eta}, \qquad g_{22} = \boldsymbol{r}_{\eta} \cdot \boldsymbol{r}_{\eta}$$

The control functions P and Q are linear combinations of the

Received April 15, 1994; presented as Paper 94-2334 at the AIAA 25th Fluid Dynamics Conference, Colorado Springs, CO, June 20–23, 1994; revision received Feb. 1, 1995; accepted for publication Feb. 2, 1995.

*Research Engineer, Institute for Aerospace Studies, 4925 Dufferin Street. Member AIAA.
†Associate Professor, Institute for Aerospace Studies, 4925 Dufferin Street. Member AIAA.

adaptive control functions P_a and Q_a and geometric control functions P_g and Q_g, as follows:

$$P = b_1 P_g + b_2 P_a$$

$$Q = b_3 Q_g + b_4 Q_a$$

where b_i are user-specified parameters.

The geometric control functions cluster points to boundaries at a user-specified off-body spacing and achieve orthogonality of the transverse grid lines at boundaries, as described in Ref. 12. The adaptive control functions are given by

$$P_a = \frac{(w_1)_\xi}{w_1} - \frac{g_{12}}{g_{22}} \frac{(w_1)_\eta}{w_1}$$

$$Q_a = -\frac{g_{12}}{g_{11}} \frac{(w_2)_\xi}{w_2} + \frac{(w_2)_\eta}{w_2}$$

where w_1 and w_2 are the weight functions for adaptation in the ξ and η coordinate directions, respectively. The weight functions have the following form:

$$w_1 = 1 + a_1 \bar{f}_1 + a_2 \bar{f}_2$$

$$w_2 = 1 + a_3 \bar{f}_3 + a_4 \bar{f}_4$$

where a_i are user-specified clustering parameters, $\bar{f}_k$ are normalized adaptation functions given by

$$\bar{f}_k = \frac{f_k - f_{k_{\min}}}{f_{k_{\max}} - f_{k_{\min}}}$$

and f_k is some measure of the solution variation.

The adaptive grid generation scheme is presently applied to C-grid configurations about airfoil sections. Streamwise adaptation to the high flow gradients at the airfoil leading edge and at shocks is achieved through an appropriate formulation of the w_1 weight function. Similarly, adaptation to high gradient regions in the boundary layer is achieved through an appropriate formulation of the w_2 weight function. Streamwise and boundary-layer adaptation can be applied independently through zero or unit values of the parameters b_2 and b_4. Excessive skewness can result from the redistribution scheme if high gradient regions are not aligned with a particular coordinate direction. However, with a C-grid topology, the boundary layer is aligned with the ξ coordinate direction, and the shocks in transonic flows are closely aligned with the η coordinate direction. Thus, grid skewness due to adaptation is not a problem for subsonic and transonic applications using C-grids.

Adaptive grid solutions are generated using a form of periodic node movement. First, an initial unadapted grid is generated, and the flow solver is run to reasonable convergence on the initial grid. An adapted grid is generated based on weight functions evaluated from the initial grid flow solution. The flow solver is then applied to the adapted grid to obtain an improved flow solution. The cycle of adaptive grid generation followed by a new flow solution is continued until the grid and solution no longer change significantly. In practice, a single application of the adaptive grid generator was used since additional applications did not result in a further reduction in numerical error. Other methods of node movement were not investigated. The computational work required to obtain an adaptive grid solution using the control function scheme is typically 10–30% greater than that required to obtain a solution with the same number of nodes without adaptation.[2,6]

As the adaptive grid equations are iteratively solved, values of the weight functions are periodically evaluated at the evolving grid points using bilinear interpolation. Interpolation is performed relatively often at the beginning of the grid generation process when grid point movement is high and relatively infrequently as the grid generator converges and grid point movement is small. The interpolation procedure is computationally expensive, and the periodic application of interpolation saves computational effort without affecting the final solution.

The weight function surfaces can be somewhat noisy depending on the smoothness of the initial grid and flow solution such that clipping and smoothing of the weight surfaces is necessary to reduce high-frequency oscillations, as suggested in Ref. 13. The clipping operation at each grid point is given by

$$w = \begin{cases} w & \text{if } w < \beta \tilde{w} \\ \tilde{w} & \text{if } w \geq \beta \tilde{w} \end{cases}$$

where $\tilde{w}$ is the average of w evaluated from the neighboring eight nodes in the grid. The suggested value of the clipping parameter β is 1.15. Smoothing is achieved by application of the following operation at each grid point:

$$w_{i,j} = \tfrac{1}{8}(w_{i-1,j} + w_{i,j-1} + w_{i+1,j} + w_{i,j+1}) + \tfrac{1}{2} w_{i,j}$$

The adaptive control function surfaces are also smoothed using this expression.

To enhance convergence of the adaptive grid generator, the control functions are initially set to zero and slowly ramped in using a damping and under-relaxation scheme.[12] Geometric control is applied at the airfoil and wake surfaces and interpolated into the interior grid using exponential decay functions of the form

$$P_g|_{i,j} = P_g|_{i,1} \exp^{-d_1(j-1)}$$

$$Q_g|_{i,j} = Q_g|_{i,1} \exp^{-d_2(j-1)}$$

where d_1 and d_2 are user-specified decay constants.

The airfoil points are held fixed except in the case of streamwise adaptation, in which the airfoil points are moved along the airfoil surface according to the iterative solution of the following one-dimensional equidistribution statement:

$$s_i = \frac{1}{2}(s_{i+1} - s_{i-1}) + \frac{1}{8}\left[\frac{w_1|_{i+1,1} - w_1|_{i-1,1}}{w_1|_{i,1}}\right](s_{i+1} - s_{i-1})$$

where s is arclength along the airfoil surface ($\eta = 1$). Linear interpolation is used to evaluate the weight function at the evolving grid points. The wake points are always held fixed. The outer boundary points are moved along the boundary curves to achieve orthogonality of the transverse grid lines.

Flow Solver

The thin-layer Navier–Stokes equations are solved numerically using the viscous transonic airfoil code ARC2D, which is described in detail in Ref. 14. Spatial derivatives are approximated using second-order centered finite difference expressions. A nonlinear scalar artificial dissipation model that combines second- and fourth-difference dissipation to control oscillations and nonlinear instability is used. That dissipation term for the ξ direction is given by

$$\nabla_\xi (T_1 \Delta_\xi Q_{i,j} - T_2 \Delta_\xi \nabla_\xi \Delta_\xi Q_{i,j})$$

with

$$T_1 = \sigma_{i+1,j} J^{-1}_{i+1,j} \epsilon^{(2)}_{i+1,j} + \sigma_{i,j} J^{-1}_{i,j} \epsilon^{(2)}_{i,j}$$

$$T_2 = \sigma_{i+1,j} J^{-1}_{i+1,j} \epsilon^{(4)}_{i+1,j} + \sigma_{i,j} J^{-1}_{i,j} \epsilon^{(4)}_{i,j}$$

$$\epsilon^{(2)}_{i,j} = \kappa_2 \Delta t \max(\Upsilon_{i+1,j}, \Upsilon_{i,j}, \Upsilon_{i-1,j})$$

$$\epsilon^{(4)}_{i,j} = \max\left[0, \kappa_4 \Delta t - \epsilon^{(2)}_{i,j}\right]$$

$$\Upsilon_{i,j} = \frac{|p_{i+1,j} - 2p_{i,j} + p_{i-1,j}|}{|p_{i+1,j} + 2p_{i,j} + p_{i-1,j}|}$$

where Δ_ξ and ∇_ξ are first-order forward and backward difference operators, respectively, σ is a spectral radius scaling, J is the Jacobian of the grid transformation, Q is the solution vector, Δt is the time step, p is the pressure, and κ_2 and κ_4 are constants. Typical values of κ_2 and κ_4 are 1.0 and 0.01, respectively. A similar term is used for the η direction.

No-slip adiabatic boundary conditions are enforced at the airfoil boundary, characteristic boundary conditions are used at outer boundaries, and a far-field circulation correction is applied at the outer boundary. The Baldwin–Lomax turbulence model is used.

Test Cases

The following six test cases of Zingg[1] are revisited in this work: 1) NACA 0012 at $M_\infty = 0.16$, $\alpha = 0$, $Re = 2.88 \times 10^6$, and transition at 0.43 chords on both surfaces; 2) NACA 0012 at $M_\infty = 0.16$, $\alpha = 6$ deg, $Re = 2.88 \times 10^6$, and transition at 0.05 and 0.80 chords on the upper and lower surfaces, respectively; 3) NACA 0012 at $M_\infty = 0.16$, $\alpha = 12$ deg, $Re = 2.88 \times 10^6$, and transition at 0.01 and 0.95 chords on the upper and lower surfaces, respectively; 4) NACA 0012 at $M_\infty = 0.70$, $\alpha = 14.9$ deg, $Re = 9 \times 10^6$, and transition at 0.05 chords on both surfaces; 5) NACA 0012 at $M_\infty = 0.55$, $\alpha = 8.34$ deg, $Re = 9 \times 10^6$, and transition at 0.05 chords on both surfaces; and 6) RAE 2822 at $M_\infty = 0.729$, $\alpha = 2.31$ deg, $Re = 6.5 \times 10^6$, and transition at 0.03 chords on both surfaces.

Results are presented for unadapted hyperbolic and elliptic grids as well as for adapted grids. Hyperbolic grids were generated using the grid generator described in Ref. 15. Elliptic grids are generated by setting the adaptive control functions to zero in the adaptive grid generator. Adapted and elliptic grids were generated using a hyperbolic grid as an initial grid such that the number of points and some of the clustering characteristics of the initial hyperbolic grid are retained by the new grids.

Hyperbolic grids are designated with two-character names composed of an upper case letter followed by a number. Unadapted elliptic grid names have an "e" preceding the corresponding hyperbolic grid name. Similarly, boundary-layer adapted grid names are preceded by a "b" and combined boundary-layer and streamwise adapted grid names with a "bp." The A6 and N6 grids have 249 points in the streamwise coordinate direction with 97 and 49 points in the coordinate direction transverse to the body, respectively. There are 201 points on the body and 24 points in the wake. Points are clustered at the leading and trailing edges with a streamwise spacing of 2×10^{-4} chords. Normal spacing at the body is 2×10^{-6} chords. The A7 and N7 grids have the same characteristics as the A6 and N6 grids, respectively, except that the normal spacing at the body is 2×10^{-7} chords. The distance to the outer boundary is 12 chords for all grids. The grid-independent results of Ref. 1 were obtained using Richardson extrapolation of the A7 grid results and the results from a grid that has twice the number of points as the A7 grid in each coordinate direction.

Parametric Studies

Parametric studies have been conducted to determine a suitable set of input parameters for both boundary-layer and streamwise adaptations. Grid N6 was used as the initial grid for all parametric studies. With this grid, flow features are moderately well resolved, but numerical errors can be quite high. Test case 1 was used for detailed boundary-layer adaptation studies and case 5 for detailed streamwise adaptation studies. Further parametric studies were conducted with all test cases for a limited set of parameters. Different parameters would be required for qualitatively different flows and grid topologies.

Boundary-Layer Adaptation

Effective boundary-layer adaptation requires an appropriate formulation of the w_2 weight function, a sufficient number of points in the η coordinate direction, and an appropriate spacing of the first grid point off the body. The parameters used for boundary-layer adaptation are listed in Table 1. Several different forms of the boundary-layer adaptation variables (f_3, f_4) were investigated, including vorticity and first and second derivatives of velocity magnitude, Mach number, and momentum magnitude. It was found that all of these measures successfully indicated the regions of high solution activity in the boundary layer, and similar results were obtained for all measures. The gradient of Mach number was selected as an effective boundary-layer adaptation parameter.

Geometric control allows the off-body spacing (Δs_b) to be specified. The off-body spacing is an important parameter related to boundary-layer resolution. A y^+ value of less than 1 is generally desirable to have at least one grid point in the laminar sublayer, where y^+ is the standard law-of-the-wall coordinate. As the off-body spacing is reduced with a fixed number of points in the grid and a smooth distribution of points, the number of points in the boundary layer is increased. A greater number of points in the boundary layer tends to decrease friction drag error due to improved boundary-layer resolution while increasing pressure drag error due to high stretching and a decrease in resolution in regions outside the boundary layer. Hence, decreasing the off-body spacing generally results in a decrease in friction drag error and an increase in pressure drag error. The relationship between overall drag error and off-body spacing is therefore dependent on the ratio of the friction and pressure drag components in the overall drag for a particular flow. An off-body spacing of 2×10^{-6} chords, which corresponds to a y^+ of about 1, yields minimum or close to minimum drag errors for all of the test cases. Lift errors are not significantly affected by off-body spacing.

Table 1 Parameters for boundary-layer adaptation (b grids)

Parameters	Values
Adaptation variables	$f_3 = \lvert\nabla M\rvert$
	no f_4
Clustering	$a_3 = 1.3 \times 10^6$, $a_4 = 0$
Control combination	$b_1 = 1, b_2 = 0$
	$b_3 = 1, b_4 = 1$
w_2 clipping	Five iterations ($\beta = 1.15$)
w_2 smoothing	Two iterations
Q_a smoothing	One iteration
Boundary treatment	Fixed airfoil points
	Fixed wake points
Geometric control	At airfoil and wake:
	$\Delta s_b = 2 \times 10^{-6}$ chords
	P_g decay: $d_1 = 0.05$
	Q_g decay: $d_2 = 0$
Postsmoothing	One iteration

The clustering parameter a_3 is estimated from the following form of the equidistribution statement:

$$w_{2_{\min}} \Delta s_{2_{\max}} = w_{2_{\max}} \Delta s_{2_{\min}}$$

where s_2 is arclength along a constant-ξ coordinate curve in the positive η coordinate direction. Since $w_{2_{\min}} = 1$, $w_{2_{\max}} = 1 + a_3$ (with $a_4 = 0$), $\Delta s_{2_{\min}}$ is the spacing at the body, and $\Delta s_{2_{\max}}$ is the spacing at the outer boundary, the following estimate for a_3 is obtained:

$$a_3 = \frac{\Delta s_{2_{\max}}}{\Delta s_{2_{\min}}} - 1$$

This expression leads to a value of $a_3 = 1.3 \times 10^6$ for the grids studied. The parameter a_3 was varied between values of 10^5 to 10^8 for all test cases and up to 10^{10} for some cases. Lift errors are not significantly affected by a_3. The friction drag error decreases and the pressure drag error increases slightly with increased a_3 due to increased clustering of points in the boundary layer. A value of 1.3×10^6 was found to yield either minimum or close to minimum drag errors for all test cases.

The weight function surface is clipped 5 times and smoothed twice, which effectively removes high-frequency oscillations. Although the solution is not highly dependent on these parameters, it is recommended that some clipping and smoothing be applied to the weight function surface. A single smoothing iteration of the adaptive control function surface was found to enhance grid convergence.

Orthogonality of the transverse grid lines at the airfoil and wake is controlled by P_g. For near-orthogonality with the boundary to extend a reasonable distance into the grid interior, a low value of d_1 is required. However, values of d_1 lower than 0.05 tend to cause oscillations in the iterative grid solution. The Q_g control function allows the off-body spacing at the airfoil and wake to be controlled. A zero value of d_2 results in a strong attraction of grid lines to the airfoil and wake, which is desirable for viscous flow computations.

An investigation of the effect of the smoothness of the adapted grid on numerical error was conducted. Smoothing of the final grid is achieved by turning off both adaptive and geometric control functions for the final grid generation iterations. Increasing the number of smoothing iterations applied to an adapted grid yields a gradual decrease in pressure drag error and has little effect on the lift error.

Table 2 Parameters for combined streamwise and boundary-layer adaptation (bp grids)

Parameters	Values
Adaptation variables	$f_1 = \lvert dp/ds_1 \rvert$
	$f_2 = \lvert d^2p/ds_1^2 \rvert$
	$f_3 = \lvert \nabla M \rvert$
	no f_4
Clustering	$a_1 = 50, a_2 = 30$
	$a_3 = 1.3 \times 10^6, a_4 = 0$
Control combination	$b_1 = 1, b_2 = 0$
	$b_3 = 1, b_4 = 1$
w_1/w_2 clipping	Five iterations ($\beta = 1.15$)
w_1/w_2 smoothing	Two iterations
P_a/Q_a smoothing	One iteration
Boundary treatment	Adaptive airfoil points
	Fixed wake points
Geometric control	At airfoil and wake:
	$\Delta s_b = 2 \times 10^{-6}$ chords
	P_g decay: $d_1 = 0.05$
	Q_g decay: $d_2 = 0$
Postsmoothing	One iteration

Friction drag error is significantly reduced by a single smoothing iteration, and further smoothing iterations result in a gradual increase in error from the single iteration level. A single postsmoothing iteration was therefore applied for all test cases.

Streamwise Adaptation

Effective adaptation to the gradients in the streamwise direction requires an appropriate formulation of the w_1 weight function and a sufficient number of points in the ξ coordinate direction. The parameters used for a combination of streamwise and boundary-layer, adaptation are listed in Table 2. The streamwise adaptation variables (f_1, f_2) were selected to be the first and second derivatives of pressure with respect to s_1, where s_1 is arclength along a constant-η coordinate curve in the positive ξ coordinate direction. This formulation senses high gradients at suction peaks as well as at shocks.

A preliminary investigation of clustering was conducted by manually changing the airfoil surface point distribution at the leading edge, trailing edge, and shock for case 5 using hyperbolic grids. The investigation showed that leading- and trailing-edge clustering affects both lift and drag errors significantly. Low drag error is generally associated with high lift error and vice versa such that a compromise is necessary in the selection of the "best" leading- and trailing-edge clustering values. Manual clustering at the known shock location indicated that shock clustering can reduce both the lift and drag errors, although the error reduction is fairly small. Excessive shock clustering leads to increased error.

The amount of clustering to regions of rapidly changing pressure is controlled in the adaptive scheme by specifying a_1. The a_2 parameter is used to cluster points to regions of high streamwise curvature of the surface pressure distribution, which is necessary for clustering points at maxima and minima of the surface pressure distribution. Several combinations of a_1 and a_2 were evaluated with $20 \leq a_1, a_2 \leq 70$. The intermediate values of $a_1 = 50$ and $a_2 = 30$ produce reasonable results. Varying a_1 and a_2 yields slight changes in lift and drag errors depending on the flow characteristics.

Streamwise adaptation is achieved through the adaptive movement of grid points on the airfoil surface. Streamwise adaptation of interior grid points is not used ($b_2 = 0$) since the change in airfoil boundary point distribution results in appropriate changes in the interior grid point distribution. The combination of streamwise adaptation on the airfoil surface and in the grid interior resulted in no solution improvement over the use of adapted airfoil points only.

Results and Discussion

Results are presented in Tables 3–8. The tables specify the numerical errors relative to the grid-independent solution given in the table captions. Grid adaptation has effectively reduced the lift and overall drag errors for most cases. Boundary-layer adaptation significantly reduces the friction drag error for all cases but has a minimal effect on the lift and pressure drag errors. Streamwise adaptation results in a significant error reduction with N6 grids for the strong shock case (case 5) but provides less significant changes for the other cases.

Table 3 Grid study for case 1: NACA 0012 at $M_\infty = 0.16$ and $\alpha = 0$ (grid-independent $C_d = 0.00579$, $C_{d_p} = 0.00080$, and $C_{d_f} = 0.00499$)

Grid	C_d,%	C_{d_p},%	C_{d_f},%
Grid size: 249 × 97			
A7	3.6	6.3	3.0
A6	13.1	6.3	14.2
eA6	12.1	8.8	12.8
bA6	0.2	7.5	−1.0
bpA6	1.0	11.3	−0.4
Grid size: 249 × 49			
N7	14.0	41.3	9.6
N6	42.1	31.3	43.7
eN6	39.4	41.3	39.1
bN6	13.3	48.8	7.6
bpN6	14.2	50.0	8.4

Table 4 Grid study for case 2: NACA 0012 at $M_\infty = 0.16$ and $\alpha = 6$ deg (grid-independent $C_l = 0.6620$, $C_d = 0.00779$, $C_{d_p} = 0.00252$, and $C_{d_f} = 0.00527$)

Grid	C_l,%	C_d,%	C_{d_p},%	C_{d_f}, %
Grid size: 249 × 97				
A7	−0.3	9.9	24.2	3.0
A6	−0.3	16.0	18.7	14.6
eA6	−0.2	13.4	13.1	13.5
bA6	0.0	4.4	11.9	0.8
bpA6	0.0	4.0	11.9	0.2
Grid size: 249 × 49				
N7	−1.2	30.7	79.4	7.4
N6	−1.3	48.9	64.3	41.6
eN6	−1.0	40.3	45.6	37.8
bN6	−0.6	21.7	50.8	7.8
bpN6	−0.8	21.7	52.4	7.0

Table 5 Grid study for case 3: NACA 0012 at $M_\infty = 0.16$ and $\alpha = 12$ deg (grid-independent $C_l = 1.3122$, $C_d = 0.01261$, $C_{d_p} = 0.00777$, and $C_{d_f} = 0.00483$)

Grid	C_l,%	C_d,%	C_{d_p},%	C_{d_f}, %
Grid size: 249 × 97				
A7	−1.3	21.0	33.6	1.0
A6	−1.1	21.4	27.0	12.8
eA6	−0.9	15.9	18.3	12.2
bA6	−0.9	11.7	18.7	0.6
bpA6	−0.7	9.1	14.8	0.2
Grid size: 249 × 49				
N7	−3.4	62.5	100.1	2.3
N6	−3.1	64.5	82.6	35.6
eN6	−2.3	46.7	54.8	33.7
bN6	−2.2	37.8	57.5	6.4
bpN6	−2.4	39.5	60.4	6.2

The error reduction is dependent on both the characteristics of the flow and the initial grid. The results of case 1, in which the drag is dominated by friction drag, show a large decrease in overall drag error for the adapted grids compared with the unadapted hyperbolic and elliptic A6 and N6 grids. The reduction in overall drag is due solely to the reduction in friction drag error. Streamwise adaptation does not improve the results for this case. Figure 1 shows a detail of the unadapted elliptic eN6 grid. The differences between the eN6 grid and the boundary-layer adapted bN6 grid are indistinguishable on the scale of Fig. 1 since redistribution predominantly affects points in the boundary layers. Figure 2 shows the nondimensional wall shear stress distribution τ_w for case 1, where τ_w is nondimensionalized by freestream density and the square of freestream speed of sound. The A7A solution is from a 497 × 193 grid that is close to the grid-independent solution. The boundary-layer adapted bN6 results predict the wall shear stress much better than the unadapted

Table 6 Grid study for case 4: NACA 0012 at $M_\infty = 0.7$ and $\alpha = 1.49$ deg (grid-independent $C_l = 0.2536$, $C_d = 0.00743$, $C_{d_p} = 0.00211$, and $C_{d_f} = 0.00532$)

Grid	C_l,%	C_d,%	C_{d_p},%	C_{d_f},%
Grid size: 249 × 97				
A7	0.4	2.3	7.6	0.2
A6	0.3	8.1	8.1	8.1
eA6	0.4	8.1	9.5	7.3
bA6	0.6	2.0	8.1	−0.4
bpA6	0.7	1.2	5.7	−0.6
Grid size: 249 × 49				
N7	−0.8	4.3	23.7	−3.4
N6	−0.7	19.5	20.9	19.2
eN6	−0.8	22.5	33.6	18.0
bN6	−0.8	10.4	37.0	−0.2
bpN6	−0.9	10.5	37.9	−0.4

Table 7 Grid study for case 5: NACA 0012 at $M_\infty = 0.55$ and $\alpha = 8.34$ deg (grid-independent $C_l = 1.0013$, $C_d = 0.03476$, $C_{d_p} = 0.03089$, and $C_{d_f} = 0.00387$)

Grid	C_l,%	C_d,%	C_{d_p},%	C_{d_f},%
Grid size: 249 × 97				
A7	−1.4	0.9	1.2	−0.8
A6	−1.5	1.2	0.2	8.5
eA6	−1.6	0.9	0.0	8.0
bA6	−1.3	0.4	0.6	−1.3
bpA6	−0.8	−1.2	−1.3	−0.3
Grid size: 249 × 49				
N7	−1.8	6.4	7.5	−2.3
N6	−1.8	7.4	5.3	24.0
eN6	−1.3	8.4	6.4	24.5
bN6	−1.5	6.8	7.5	1.8
bpN6	−0.6	5.2	5.3	4.4

Table 8 Grid study for case 6: RAE 2822 at $M_\infty = 0.729$ and $\alpha = 2.31$ deg (grid-independent $C_l = 0.7950$, $C_d = 0.01336$, $C_{d_p} = 0.00815$, and $C_{d_f} = 0.00522$)

Grid	C_l,%	C_d,%	C_{d_p},%	C_{d_f},%
Grid size: 249 × 97				
A7	−0.7	2.9	4.5	0.2
A6	−0.6	4.6	3.6	5.9
eA6	−0.7	5.2	4.8	5.6
bA6	−0.8	1.9	2.9	0.2
bpA6	−1.0	1.0	1.7	−0.4
Grid size: 249 × 49				
N7	−1.8	7.8	15.3	−4.4
N6	−1.8	11.5	10.9	11.9
eN6	−2.2	16.0	18.5	11.9
bN6	−1.9	12.6	20.7	−0.4
bpN6	−2.1	13.4	22.6	−1.1

N6 result. The adapted grid results are particularly good at the suction peak and in the turbulent boundary-layer region. Although the bN6 grid results are only slightly better than the N7 grid results, the bA6 grid results are significantly better than the A7 grid results, indicating that a larger number of points increases the effectiveness of adaptation. The N7 grid results are particularly good for case 1 since the N7 grid has low friction drag error due to the relatively large number of points in the boundary layer.

In contrast, the N7 grid errors are relatively large for cases 2 and 3 since the pressure drag contribution to overall drag is more significant. The results for cases 2 and 3 again show a large reduction in friction drag error due to boundary-layer adaptation. Streamwise adaptation does not improve the results for these cases. The errors in drag for case 3 are relatively high even with grid redistribution due to the difficult nature of the flow, which is separated on the upper surface at about 96% chord.

The flow in case 4 is transonic with a weak shock on the upper surface. A comparison of the results for similar grids shows that adaptation has resulted in a significant decrease in the overall drag

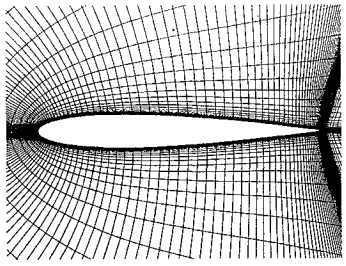

Fig. 1 eN6 grid about the NACA 0012 airfoil section.

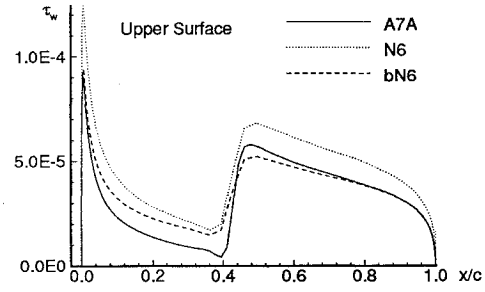

Fig. 2 Nondimensional wall shear stress on the airfoil surface for case 1.

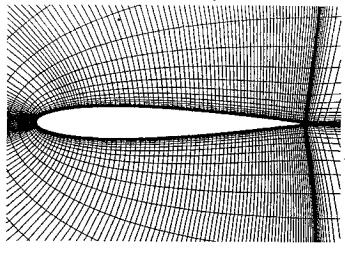

Fig. 3 bpN6 grid for case 5.

error. However, the N7 overall drag error is less than the adapted bN6 and bpN6 overall drag errors since the hyperbolic grid results have lower pressure drag errors than the elliptic and adapted grids for this case.

Case 5 is a transonic flow case with a strong shock on the upper surface at 13% chord, a small separated flow region after the shock, and final flow separation at about 90% chord. The friction drag error for case 5 is significantly reduced by boundary-layer adaptation, but the resulting reduction in the overall drag level is small since the drag is dominated by pressure drag. The combination of boundary layer and streamwise adaptation reduces error levels for grid N6. The error reduction is much larger than that obtained through manual shock clustering. The combination of boundary-layer and streamwise adaptation reduces the errors in lift and friction drag for the A6 grids, but an overshoot in pressure drag reduction leads to an overall drag increase over the bA6 grid level. Figure 3 shows a detail of the bpN6 grid, which is adapted to both the boundary-layer and streamwise gradients. The clustering of points on the upper surface at 13% chord corresponds to the position of the strong shock. The shock clustering is only slight, but increasing the shock clustering beyond this level results in increased numerical errors. The solution improvement due to shock clustering can be clearly seen in Fig. 4, which shows the nondimensional wall shear stress distribution. No effort has been made to cluster nodes in the transition region at 5% chord, since the present flow solver does not model transitional flow.

Case 6 is a transonic flow with a weak shock about the RAE 2822 airfoil section. The results are similar to case 4, which is also a weak shock case.

Numerical errors in Navier–Stokes computations are dependent on the artificial dissipation added to the numerical scheme.[16,17] A matrix dissipation model[18] or an upwind scheme can be used to reduce the numerical errors due to dissipation. A brief study was conducted to demonstrate that a reduced level of artificial dissipation combined with grid adaptation results in a complementary reduction

Table 9 Dissipation study for case 4

Grid	κ_2	κ_4	C_l, %	C_d, %	C_{d_p}, %	C_{d_f}, %
N6	1.0	0.01	−0.7	19.5	20.9	19.2
eN6	1.0	0.01	−0.8	22.5	33.6	18.0
eN6	0.0	0.005	0.1	10.6	13.7	9.4
bpN6	1.0	0.01	−0.9	10.5	37.9	−0.4
bpN6	0.0	0.005	0.3	3.9	14.7	−0.4

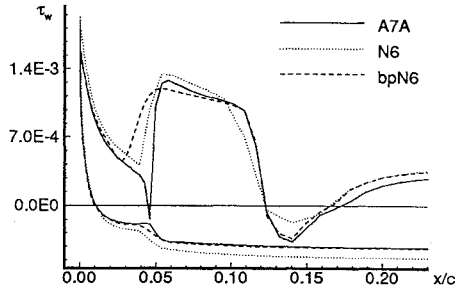

Fig. 4 Nondimensional wall shear stress on the airfoil surface for case 5.

in numerical error. The results of Tables 3–8 have been generated using dissipation constants of $\kappa_2 = 1.0$ and $\kappa_4 = 0.01$ in each coordinate direction. It is possible to lower the values of κ_2 and κ_4 and still obtain convergent oscillation-free solutions, especially for cases without strong shocks. Lower values of κ_2 and κ_4 reduce the level of contamination of the solution by artificial dissipation, and numerical errors are reduced. The numerical error reduction due to lowering κ_2 and κ_4 for case 4 are shown in Table 9. These results are typical of the results obtained for all test cases. Although case 4 is a transonic flow, the shock is very weak, and second-order dissipation is not required. The usual value of κ_4 was halved, and this new combination of κ_2 and κ_4 results in a convergent and oscillation-free solution. Note from the table that the numerical errors are reduced at the new level of artificial dissipation, and the combination of reduced artificial dissipation and grid adaptation is beneficial.

Conclusions

The adapted grid is a compromise between the requirements of grid smoothness and skewness and the need to cluster in regions of high solution gradients. Consequently, the error reduction due to grid adaptation is sensitive to the adaptive grid generation parameters used, especially those affecting the smoothness of the adapted grid. Some of the characteristics of the initial grid, such as the number of grid points in each coordinate direction, introduce further constraints. These constraints are a shortcoming of the grid redistribution approach as opposed to the grid enrichment approach. The advantage of grid redistribution is the retention of a structured database with its associated benefits. An improved approach would include the capability of altering the number of points in each coordinate direction based on the solution while retaining the topology of the original grid.

In general, the gains due to adaptive redistribution are modest, especially if the additional 10–30% computational cost is considered. Numerical errors in friction drag are consistently and significantly reduced by boundary-layer adaptation, but the error reduction in pressure drag and lift is not as large. The limited reduction in numerical error is partly due to the selection of good initial grids; less appropriate initial grids would result in greater gains due to redistribution. Excessively poor initial grids, however, would result in poor adapted grids due to the dependence of the adapted grid on the initial grid characteristics. Redistribution may also be more effective for unsteady flows in which the high gradient regions are moving. Most of the cases in this study produce lower numerical errors in drag with an adapted grid than with an unadapted grid with 10–30% more nodes. This leads to the recommendation that adaptive redistribution should be applied if minimizing the numerical error in drag for a given number of grid points is particularly important.

Acknowledgment

This work was sponsored by Defence Research Establishment Suffield of Canada.

References

[1]Zingg, D. W., "Grid Studies for Thin-Layer Navier–Stokes Computations of Airfoil Flowfields," *AIAA Journal*, Vol. 30, No. 10, 1992, pp. 2561–2564.

[2]Dannenhoffer, J. F., "A Comparison of Adaptive-Grid Redistribution and Embedding for Steady Transonic Flows," AIAA Paper 90-1565, June 1990.

[3]Davies, C. B., and Venkatapathy, E., "Application of a Solution Adaptive Grid Scheme to Complex Three-Dimensional Flows, " *AIAA Journal*, Vol. 30, No. 9, 1992, pp. 2227–2233.

[4]Warren, G. P., Anderson, W. K., Thomas, J. L., and Krist, S. L., "Grid Convergence for Adaptive Methods," AIAA Paper 91-1592, June 1991.

[5]Eiseman, P. R., "Adaptive Grid Generation," *Computer Methods in Applied Mechanics and Engineering*, Vol. 64, Oct. 1987, pp. 321–376.

[6]Kim, H. J., and Thompson, J. F., "Three-Dimensional Adaptive Grid Generation on a Composite-Block Grid," *AIAA Journal*, Vol. 28, No. 3, 1990, pp. 470–477.

[7]Catherall, D., "Solution Adaptivity with Structured Grids," *Numerical Methods for Fluid Dynamics*, edited by M. J. Baines and K. W. Morton, Clarendon, Oxford, England, UK, 1993, pp. 19–37.

[8]Brackbill, J. U., and Saltzman, J. S., "Adaptive Zoning for Singular Problems in Two Dimensions," *Journal of Computational Physics*, Vol. 46, June 1982, pp. 342–368.

[9]Holcomb, J. E., "Requirements for the Adaptive Grid Navier–Stokes Analysis of Complex 3-D Configurations and Flowfields," *Numerical Grid Generation in Computational Fluid Dynamics '88*, edited by S. Sengupta, J. Häuser, P. R. Eiseman, and J. F. Thompson, Pineridge, Swansea, Wales, UK, 1988, pp. 495–504.

[10]Hall, D. J., and Zingg, D. W., "An Adaptive Grid Generator for Structured Grids," Univ. of Toronto Inst. for Aerospace Studies, Downsview, Ontario, Canada, Technical Rept., Dec. 1992.

[11]Thompson, J. F., Warsi, Z. U. A., and Mastin, C. W., *Numerical Grid Generation, Foundations and Applications*, North-Holland, Amsterdam, 1985.

[12]Sorenson, R. L., "A Computer Program to Generate Two-Dimensional Grids About Airfoils and Other Shapes by the Use of Poisson's Equation," NASA TM 81198, 1980.

[13]Bockelie, M. J., and Eiseman, P. R., "A Time-Accurate Grid Method and the Numerical Simulation of a Shock-Vortex Interaction," NASA TM 2998, June 1990.

[14]Pulliam, T. H., "Efficient Solution Methods for the Navier–Stokes Equations," *Lecture Notes for the Von Kármán Institute for Fluid Dynamics Lecture Series: Numerical Techniques for Viscous Flow Computations in Turbomachinery Bladings*, Von Kármán Inst. for Fluid Dynamics, Brussels, Belgium, Jan. 1986.

[15]Barth, T. J., Pulliam, T. H., and Buning, P. G., "Navier–Stokes Computations for Exotic Airfoils," AIAA Paper 85-0109, Jan. 1985.

[16]Reddy, S., and Papadakis, M., "Artificial Viscosity Models for the Navier–Stokes Equations and Their Effect in Drag Prediction," AIAA Paper 93-0193, Jan. 1993.

[17]Varma, R. R., and Caughey, D. A., "Evaluation of Navier–Stokes Solutions Using the Integrated Effect of Numerical Dissipation," *AIAA Journal*, Vol. 32, No. 2, 1994, pp. 294–300.

[18]Turkel, E., and Vatsa, V. N., "Effect of Artificial Viscosity on Three-Dimensional Flow Solutions," *AIAA Journal*, Vol. 32, No. 1, 1994, pp. 39–45.